The F-BAR protein Cip4/Toca-1 antagonizes the formin Diaphanous in membrane stabilization and compartmentalization

Shuling Yan[1,*], Zhiyi Lv[1,*], Moritz Winterhoff[2,*], Christian Wenzl[1], Thomas Zobel[3], Jan Faix[2], Sven Bogdan[3,‡] and Jörg Grosshans[1,‡]

[1]Institut für Biochemie, Universitätsmedizin, Universität Göttingen, Justus-von-Liebig Weg 11, 37077 Göttingen, Germany
[2]Institut für Biophysikalische Chemie, Medizinische Hochschule Hannover, Carl-Neuberg Strasse 1, 30625 Hannover, Germany
[3]Institut für Neurobiologie, Universität Münster, Badestrasse 9, 48149 Münster, Germany

*These authors contributed equally to this work
‡Authors for correspondence (jgrossh@gwdg.de; sbogdan@uni-muenster.de)

Accepted 1 February 2013
Journal of Cell Science 126, 1796–1805

doi: 10.1242/jcs.118422

Summary

During *Drosophila* embryogenesis, the first epithelium with defined cortical compartments is established during cellularization. Actin polymerization is required for the separation of lateral and basal domains as well as suppression of tubular extensions in the basal domain. The actin nucleator mediating this function is unknown. We found that the formin Diaphanous (Dia) is required for establishing and maintaining distinct lateral and basal domains during cellularization. In *dia* mutant embryos lateral marker proteins, such as Discs-large and Armadillo/β-Catenin spread into the basal compartment. Furthermore, high-resolution and live-imaging analysis of *dia* mutant embryos revealed an increased number of membrane extensions and endocytic activity at the basal domain, indicating a suppressing function of *dia* on membrane invaginations. Dia function might be based on an antagonistic interaction with the F-BAR protein Cip4/Toca-1, a known activator of the WASP/WAVE-Arp2/3 pathway. Dia and Cip4 physically and functionally interact and overexpression of Cip4 phenocopies *dia* loss-of-function. *In vitro*, Cip4 inhibits mainly actin nucleation by Dia. Thus, our data support a model in which linear actin filaments induced by Dia stabilize cortical compartmentalization by antagonizing membrane turnover induced by WASP/WAVE-Arp2/3.

Key words: *Drosophila*, F-BAR, Formin, Embryogenesis, Membrane compartment

Introduction

In early *Drosophila* embryogenesis the first polarized cells are formed during cellularization immediately following the last nuclear division, when the plasma membrane invaginates between adjacent nuclei and generates a network of furrows with furrow canals (FC) at its leading edge. During invagination the membrane polarizes forming distinct basal and lateral domains (Lecuit and Wieschaus, 2000). The basal domain comprises the FC. The FC membrane is highly dynamic in the initial phase of cellularization forming micrometer long tubules extending from the basal domain into the cytoplasm (Sokac and Wieschaus, 2008a). After about 5–10 minutes, the tubular extensions disappear indicating a stabilization of the FC membrane. Concomitantly with polarization and membrane stabilization, F-actin accumulates at the FC. Drug treatment showed that F-actin is required to maintain membrane polarization and stabilization (Sokac and Wieschaus, 2008a; Sokac and Wieschaus, 2008b). However, the actin nucleator responsible for these functions has not been identified yet.

The formin Diaphanous (Dia) represents a likely candidate. Formins control membrane-associated F-actin and membrane dependent processes and structures such as contractile ring in cytokinesis, endosomal dynamics, phagocytosis as well as protrusions such as filopodia and lamellipodia (Chesarone et al., 2010). In *Drosophila* embryos, Dia functionally associates with the cytokinetic furrow (Castrillon and Wasserman, 1994), with mitotic pseudocleavage furrow in syncytial embryos and the furrow canal during cellularization (Afshar et al., 2000; Padash Barmchi et al., 2005; Grosshans et al., 2005), cell contacts during cell intercalation (Levayer et al., 2011), with adherens junctions in the epidermis (Homem and Peifer, 2008) and controls apical secretion (Massarwa et al., 2009). The activity of Dia is controlled by Rho1 (also called RhoA) that releases an autoinhibitory intramolecular interaction (Li and Higgs, 2003; Grosshans et al., 2005). In addition to RhoGTPases, as yet unidentified membrane-associated factors are most likely involved in regulation of Dia (Faix and Grosse, 2006; Chesarone et al., 2010; Seth et al., 2006).

A molecular link between the membrane and actin dynamics is provided by proteins of the F-BAR family, such as Cip4/Toca-1 (Heath and Insall, 2008; Robertson et al., 2009; Aspenström, 2010; Fricke et al., 2010). Cip4/Toca-1 binds to membranes with high curvature and recruits activators of the Arp2/3 complex such as SCAR/WAVE and WASP with its C-terminal SH3 domain to promote local accumulation of branched actin filaments (Fricke et al., 2009). Arp2/3-induced branched actin filaments play important functions in membrane-dependent processes including

membrane protrusions, vesicle rocketing and movement, cell junctions and endocytosis (Campellone and Welch, 2010; Suetsugu and Gautreau, 2012). Although members of the F-BAR family can clearly affect actin regulators and the structure of phospholipid membranes in various experimental situations, their physiological function is less obvious possibly due to genetic redundancy (Fricke et al., 2010; Roberts-Galbraith and Gould, 2010).

In this study, we identify Dia as an actin nucleator responsible for F-actin formation in compartmentalization and membrane stabilization during cellularization. Furthermore, we reveal and characterize a direct and antagonistic interaction of Dia with the F-BAR protein Cip4.

Results

Lateral marker proteins are not excluded from the furrow canal in *dia* mutants

During the initial phase of cellularization, the basal and lateral cortical domains of the plasma membrane are established and maintained (Lecuit and Wieschaus, 2000). The basal domain comprises the FC, the lateral domain and the furrow (Fig. 1A). Some markers, such as Discs-large (Dlg), Armadillo (Arm, *Drosophila* homologue of β-catenin), Patj and Slam are exclusively found in either the lateral or basal domain, whereas others such as RhoGEF2, Dia or F-actin are strongly enriched in the basal domain (Fig. 1A–C; Grosshans et al., 2005). To test whether Dia is involved in establishing or maintaining the cortical compartments, we stained embryos from *dia* germline clones (in the following called *dia* embryos) for lateral and basal markers. In contrast to wild-type embryos, the lateral marker Dlg spread into the basal domain where it overlapped with Patj (Fig. 1D,F). The overlap with FC markers was detected throughout cellularization, including mid and late stages, when the FC has passed through the nuclear layer. Similar to Dlg, the junctional marker Arm stained the FC as shown by the overlap with Slam (Fig. 1E,G). To assess the specificity of the phenotype we analyzed embryos mutant for *Abl*, encoding the non-receptor tyrosine kinase Abelson that regulates F-actin organization in the early embryo (Grevengoed et al., 2003). With respect to Dlg and Slam distribution we found no differences between *Abl* mutant and wild-type embryos (Fig. 1H), showing that Dia controls specific aspects of F-actin formation at the FC. In contrast to Dlg and Arm, Slam and Patj remained restricted to the basal domain in wild-type and *dia* embryos, suggesting that Dia is not essential for defining or maintaining the identity of the basal domain. In summary, our data show that Dia is required for exclusion of lateral markers from the furrow canal and thus for separating lateral and basal cortical domains.

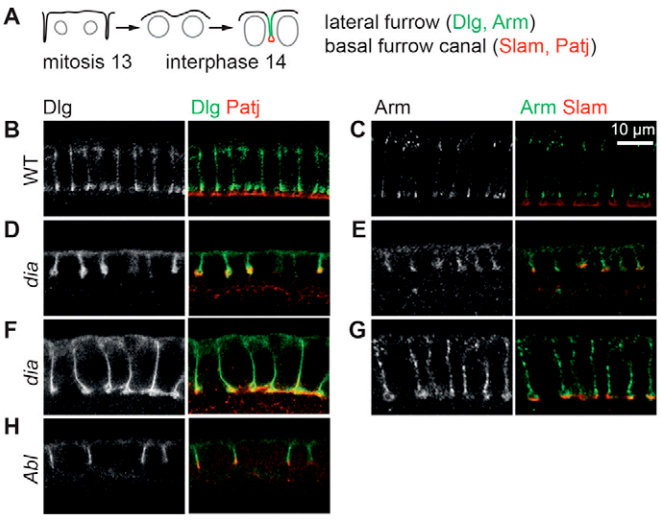

Fig. 1. Dia is required for exclusion of lateral markers from the basal domain. (**A**) Drawing of furrow invagination and formation of lateral and basal domains in mitosis 13 and interphase 14/cellularization. (**B–H**) Wild-type (B,C), *dia[SY5]* (D,E early cellularization; F,G late cellularization) and *abl* (H) embryos were fixed and stained for Dlg (white/green), Patj (red), Arm (white/green) and Slam (red) as indicated. Scale bar: 10 µm.

Persistent tubular membrane invaginations in *dia* mutants

During cellularization the invaginating plasma membrane is initially highly dynamic but stabilizes after about 5–10 minutes (Fig. 2A). The dynamic membrane is characterized by long tubular extensions that are labelled by the N-BAR protein Amphiphysin (Amph; Zelhof et al., 2001; Sokac and Wieschaus, 2008a). The tubular extensions are only transiently visible. When the furrow forms and F-actin accumulates at the FC after about 5–15 minutes in interphase 14, the tubular extensions disappear (Sokac and Wieschaus, 2008a). F-actin is required for this stabilization of the membrane, since treatment of embryos with Cytochalasin leads to persisting long tubular extensions (Sokac and Wieschaus, 2008a). To test a function of Dia in the stabilization of the FC, we characterized Amph staining in *dia* embryos by conventional and high-resolution STED microscopy (Fig. 2B,C). In contrast to conventional confocal microscopy showing uniform staining, a dotted distribution of Amph along the tubular extensions was detected by high-resolution STED microscopy. We did not observe an obvious difference of the dotted pattern and tubular length in wild-type and *dia* embryos. Analyzing the tubular extensions in relation to progression of cellularization, we found that Dia is required for suppression of the tubular extensions after the furrow has formed. In mid and late stage cellularization when almost no Amph marked membrane tubules were observed in wild-type embryos, one third of the FC were still associated with long Amph tubules in *dia* embryos (Fig. 2D). These data show that Dia is required for suppression of tubular membrane extensions at the basal compartment.

To analyze the dynamics of the tubular extensions, we explored embryos expressing the FC-specific marker GFP-slam (Wenzl et al., 2010). Time-lapse recordings of embryos expressing GFP-slam showed dynamic tubular extensions with a life time in the range of minutes (Fig. 2E; supplementary material Movies 1, 2). In wild-type embryos, these tubular extensions were observed only during the first 5 to 10 minutes of cellularization. In contrast, dynamic extensions of the FC frequently formed even at later stages of cellularization in *dia* embryos. Beside this specific marker of the FC, we observed the uptake of fluorescently labelled wheat germ agglutinin, injected into extracellular perivitteline space. Incorporation of labelled WGA was not restricted to the FC, occurring all along the furrow. Comparing the time course of the number of fluoresent punctae in wild-type and *dia* embryos, we found no obvious difference, suggesting that *dia* has no crucial function in general endocytosis (supplementary material Fig. S1; Movies 3, 4). Taken together these experiments demonstrate that Dia suppresses tubular

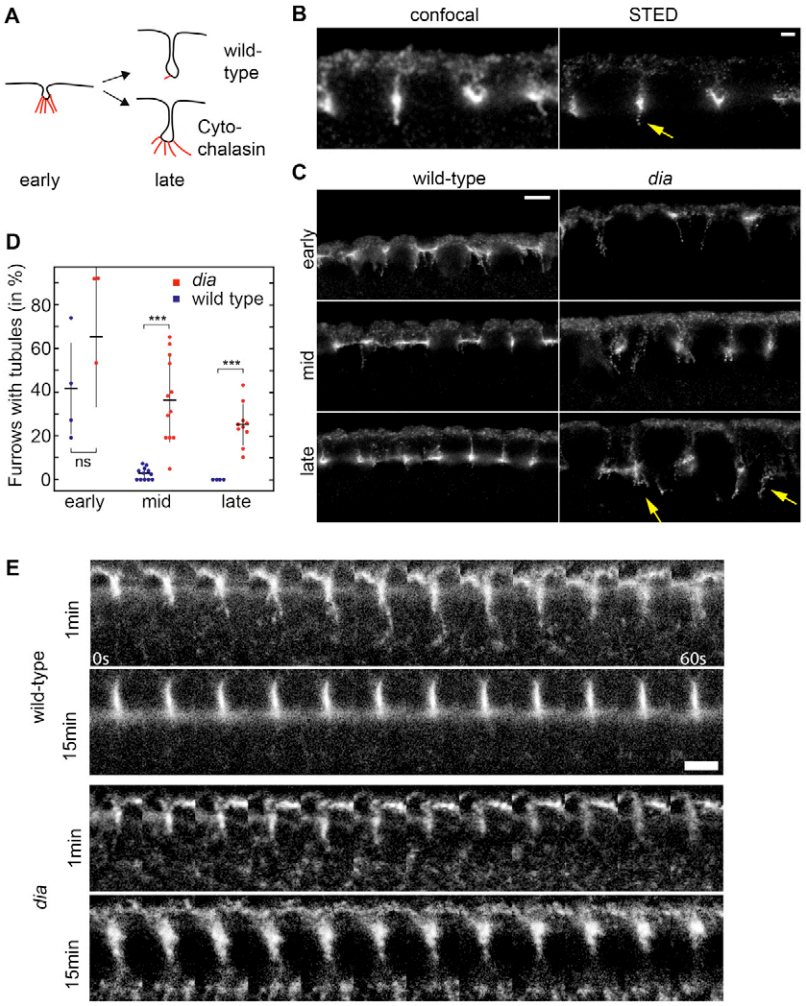

Fig. 2. Tubular extensions of the basal membrane persist throughout cellularization in *dia* mutants. (**A**) Drawing of dynamics of Amphiphysin (Amph)-labelled tubules at the furrow canal in wild-type and cytochalasine-treated embryos. (**B**) Conventional confocal and STED image of a fixed wild-type embryo stained for Amph. Arrow points to a tubular extension with a dotted Amph staining. (**C**) STED images of wild-type and *dia[SY5]* embryos in early and mid-stage cellularization. Note that in wild-type embryos the tubular extensions at the FC are present only in early stage. Arrows point to tubular extensions in latter stages of cellularization. (**D**) Quantification of tubular dynamics. Proportion of furrows with Amph-labelled tubules in fixed wild-type and *dia[SY5]* embryos. Student's *t*-test; ns (not significant; $P>0.01$), ***$P<0.0001$, i.e. for wild-type compared with *dia[SY5]* embryos, $P=0.36$ (early), $P=8.4\times10^{-5}$ (mid) and $P=1.6\times10^{-5}$ (late). Error bars indicate s.d. (**E**) Images from time-lapse recordings at onset (1 minute) and mid-stage (15 minutes) cellularization of wild-type and *dia[SY5]* embryos expressing GFPslam. Female genotypes: mat67-GAL4; UASp-GFPslam and *dia* Frt2L, mat67-GAL4/ovoD2L Frt2L; UASp-GFPslam/+. Focal depth, about 50 µm; frame rate, 1/5 seconds. Scale bars: 1 µm (B), 5 µm (C,E).

extensions and thus controls the stabilization of the FC membrane during cellularization.

The F-BAR protein Cip4 directly binds Dia and antagonizes Dia function during cellularization

How might Dia be controlled to stabilize FC membranes? F-BAR proteins are involved in coupling actin dynamics with the membrane (Heath and Insall, 2008; Robertson et al., 2009; Aspenström, 2010; Fricke et al., 2010). Interestingly, members of the Cip4 subfamily of F-BAR proteins in mammals such as Cip4 and FBP17 have been originally identified as Formin-binding proteins (Chan et al., 1996; Aspenström et al., 2006). We have recently found that Cip4, the only member of the Cip4 subfamily in *Drosophila*, integrates membrane and actin dynamics through WASP and SCAR/WAVE proteins (Fricke et al., 2009). This prompted us to test whether Dia and Cip4 physically interact in *Drosophila*. We first performed a pulldown assay with total lysates from cultured Drosophila Schneider (S2R+) cells. Dia as well as WAVE/SCAR were specifically pulled down with GST-Cip4 bound to beads (Fig. 3A) (Fricke et al., 2009). Immunoprecipitation experiments confirmed a specific interaction of Dia and GFP-Cip4. Following expression of GFP-Cip4 in *Drosophila* S2 cells and immunoprecipitation with GFP antibodies, endogenous Dia was specifically detected in the bound fraction (Fig. 3B). Finally, we reconstituted a direct interaction of Dia and Cip4 with purified proteins. Applying increasing amounts of ZZ-DiaC, a fusion protein of the ZZ (proteinA) tag and the C-terminal half of Dia including the FH1 and FH2 domains (supplementary material Figs S3, S4), we found specific binding to GST-Cip4 but not to GST alone (Fig. 3C).

We next investigated the functional relationship of the Cip4-Dia interaction during cellularization. Cip4 colocalizes with Dia at the plasma membrane including the FC where Dia is present (Fig. 4A) (Grosshans et al., 2005). Both proteins localize independently of each other, since Dia and Cip4 staining patterns are not obviously altered in the respective mutant embryos (Fig. 4B,C). *Cip4* deficient embryos do not show defects in cellularization (data not shown) and develop normally, what may be due to redundant functions with other F-BAR family members (Fricke et al., 2009; Giuliani et al., 2009; Kovacevic et al., 2012). To assess a potential function of *Cip4*, we first generated *dia ΔCip4* double mutant embryos and analyzed the domain separation and the presence of tubular extensions stained by Amph (Fig. 4D). In these embryos, tubular membrane extensions at the furrow canal were detected even in later stages. Similar to *dia* embryos, Dlg spread into the basal domain. We did not observe an obvious suppression or enhancement of the *dia* phenotype. Secondly, Cip4 was overexpressed. We found that Cip4 induced cellularization

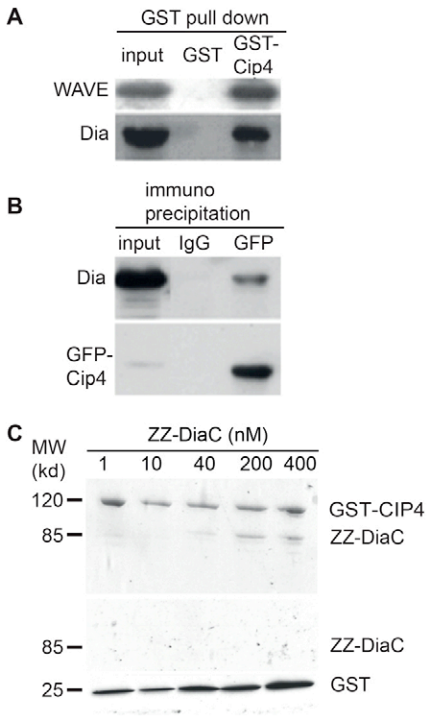

Fig. 3. Cip4 interacts with Dia. (**A**) Pulldown assay with S2R+ cell extracts using GST-Cip4 or GST bound to beads. The input and bound fractions were analyzed by immunoblotting for presence of WAVE and Dia. (**B**) Co-immunoprecipitation experiments with extracts from S2R+ cells expressing Cip4-GFP by either GFP antibody or control IgG. Input and bound fractions were analysed by immunoblotting for GFP and Dia. (**C**) Binding test with ZZ-DiaC (aa 519–1073) at indicated concentrations and GST-Cip4 or GST beads. The bound fractions were analysed by SDS polyacrylamide electrophoresis and Coomassie Blue staining.

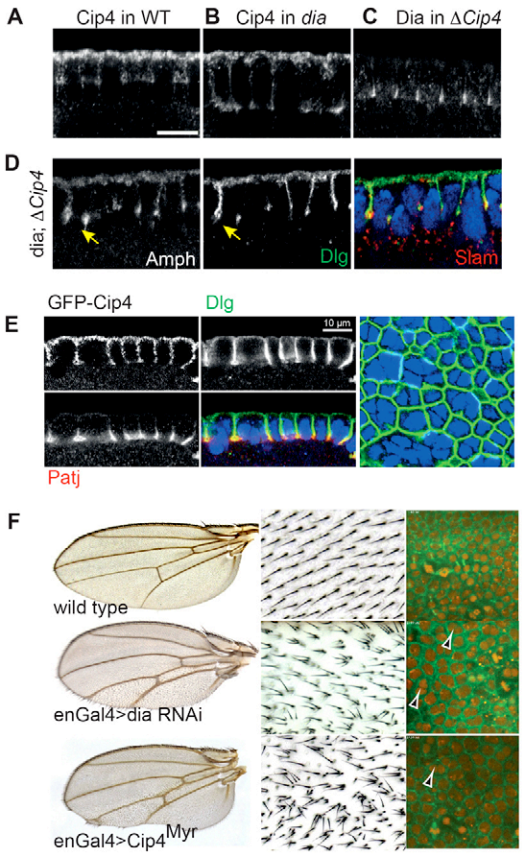

Fig. 4. *Cip4 dia* antagonism. (**A–C**) Wild-type (A), *dia[SY5]* (B) and Δ*Cip4* deficiency (C) embryos stained for Cip4 (A,B) or Dia (C). (**D**) Fixed *dia[SY5]*; Δ*Cip4* embryo stained for Amph (white), Dlg (white/green), Slam (red) and DAPI (blue). Yellow arrows point to tubular extensions (Amph channel) and furrow canal with Dlg staining. (**E**) Wild-type embryos and embryos expressing Cip4-GFP (white) were fixed and stained in a mixture for Dlg (white, green), Patj (white, red) and DNA (blue). The genotype of the embryos was identified by their Cip4-GFP fluorescence. Surface view with Dlg (green) and DNA (blue) staining shows formation of multinuclear cells. (**F**) Wings of flies expressing Cip4(Myr) and *dia* RNAi in the posterior compartment of larval and pupal wing imaginal discs. A section of the posterior compartment with the wing hair pattern is shown at higher magnification (middle panel). Cells and nuclei of living larval imaginal discs with the indicated genotype are shown by expression of Histone2Av-RFP (red) and Tubulin-GFP (green, right panel). Arrowheads point to binucleate cells. Scale bars: 10 µm.

defects similar to those seen in *dia* mutants. In such embryos, the lateral protein Dlg was not excluded from the basal domain, as indicated by the overlap with Patj, and multinuclear cells formed (Fig. 4E). This activity depends on the SH3 domain of Cip4, since expression of Cip4ΔSH3-GFP did not impair lateral and basal domain separation in the furrow and did not interfere with cellularization (supplementary material Fig. S2).

The antagonizing functions of Cip4 and Dia were not restricted to the early embryo. Both overexpression of *Cip4* and depletion of *dia* by RNAi in wing epithelia strongly induced cytokinesis defects (Fig. 4F). Differentiated wings displayed a multiple wing hair phenotype that is based on multiple trichomes per cell and is characteristic for polyploid or polynucleoid cells. Live imaging of larval imaginal discs directly showed the impaired cytokinesis (Fig. 4F; supplementary material Movies 5–7). Thus, these data show that *Cip4* antagonizes *dia in vivo*.

Cip4 is known to promote Arp2/3-dependent actin polymerization (Fricke et al., 2009). To test whether the antagonism of Cip4 and Dia involves Arp2/3-induced F-actin, we reduced Arp2/3 activity by injection of the Arp2/3 inhibitor CK666 (Nolen et al., 2009) in wild-type and *dia* embryos and by reduction of *Arp3* gene dose (Fig. 5). Injection of the Arp2/3 inhibitor CK666 led to a reduced number of Amph-stained tubules in wild type at the onset of cellularization. In contrast, injection of CK666 into *dia* embryos did not reduce the number of tubular extensions. Furthermore, reduction of the *Arp3* gene dose in *Arp3* heterozygous embryos led to a significant reduction in the number of tubular extensions as compared to wild-type embryos. Both experiments indicate that the formation or stability of tubular extensions involves Arp2/3 and that *dia* counteracts this activity.

Cip4 recruits Dia to membrane tubules

We next analyzed the functional interaction between Cip4 and Dia at the cellular and molecular level in more detail. As recently shown, Cip4 tubulates membranes and localizes at highly dynamic vesicles in cultured Drosophila S2R+ cells (Fricke et al., 2009). To explore the localization and the dynamics of Cip4 and Dia we co-expressed a series of mCherry tagged Cip4

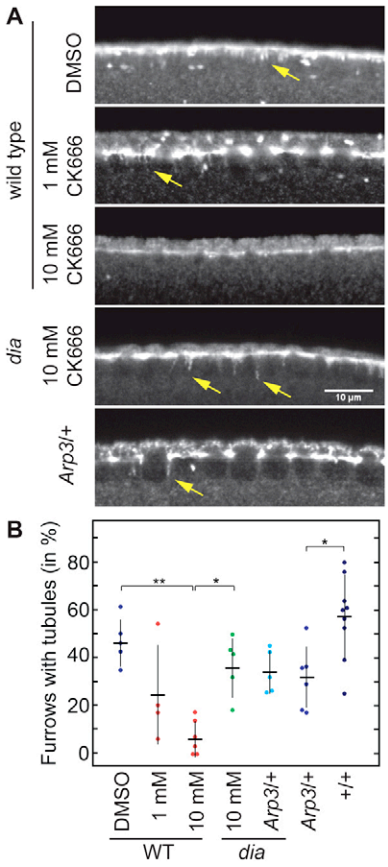

Fig. 5. Role of Arp2/3-dependent F-actin at the furrow canal. (**A**,**B**) Fixed embryos at the onset of cellularization were stained for Amph. Genotypes and injection conditions are indicated. Except for Arp3/+, embryos were injected with DMSO or Arp2/3 inhibitor CK666 at 1 mM or 10 mM. (A) Images with Amph staining. Yellow arrows point to Amph tubules. (B) Quantification of tubular extensions, showing proportion of furrows with Amph-labelled tubules. Student's *t*-test; $*P<0.01$, $**P<0.001$, i.e. $P=1.1\times10^{-4}$ for WT-DMSO compared with WT-10 mM CK666; $P=2.9\times10^{-3}$ for WT-10 mM CK666 compared with *dia*-10 mM CK666 and $P=6.9\times10^{-3}$ for WT compared with Arp3/+. Error bars indicate s.d.

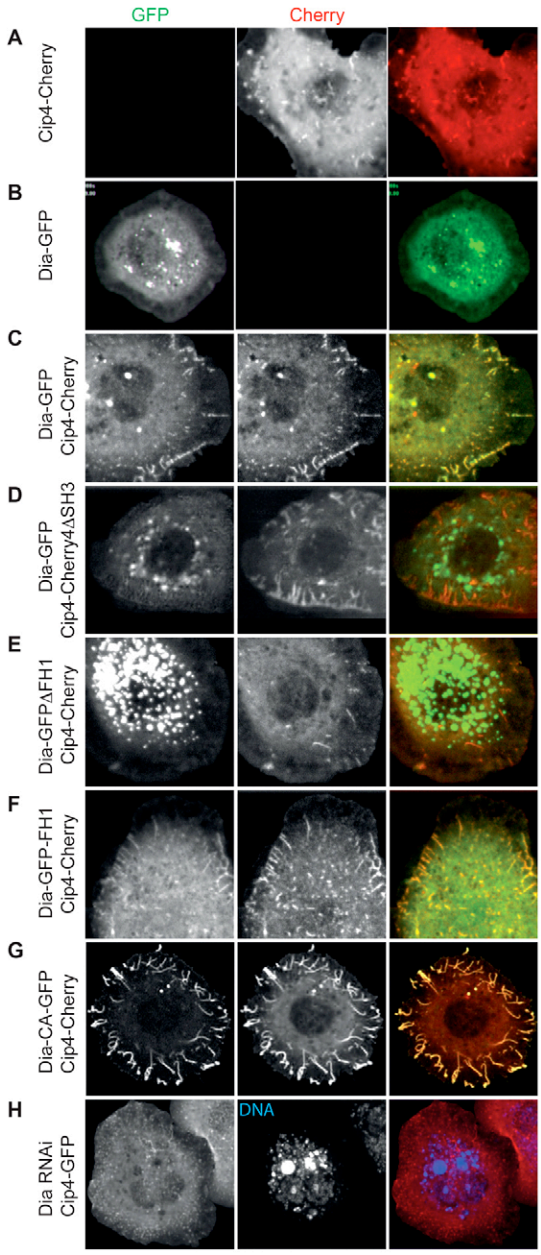

Fig. 6. Cip4-Dia colocalization in S2 cells involves FH1 and SH3 domains. (**A–G**) Images from time-lapse recordings of S2 cells expressing indicated GFP- or Cherry-tagged Dia (white, green) and Cip4 (white, red) constructs, respectively. (H) Images from time-lapse recording of S2 cells expressing Cip4-Cherry and depleted for *dia* by RNAi. Efficiency of *dia* depletion is indicated by the multinuclear phenotype, as shown by DNA staining (Hoechst, middle panel). Single-colour channels and the merged images are shown.

and EGFP tagged Dia proteins (Fig. 6A–H; supplementary material Movies 8–14). Full-length Dia-GFP was uniformly distributed in the cytoplasm of S2R+ cells (Fig. 6B; supplementary material Movie 8). However, Cip4 co-expression caused Dia to relocalize to the Cip4-mCherry-labelled membrane tubules and vesicles (Fig. 6C). Using a series of truncations we mapped the domains mediating the membrane recruitment of Dia, revealing that the SH3 domain of Cip4 and the FH1 domain of Dia are required and the proline rich FH1 domain, sufficient for mutual binding (Fig. 6D–F). In the cases of GFP-DiaΔFH1 and Cip4ΔSH3-mCherry, that lost the colocalization, we observed a weak colocalization signal, which may be due to multimerization with endogenous proteins or additional weak interaction domains. We also tested whether the Cip4-labelled tubules were affected by activation or depletion of Dia. Expression of a constitutively activated form of Dia (GFP-DiaΔDAD) stabilized the Cip4-induced tubules and reduced budding (Fig. 6G; supplementary material Movie 13) indicating that Dia counteracts Cip4-induced membrane dynamics. In contrast, depletion of *dia* by RNAi did not significantly change the dynamics of Cip4-induced vesicles and tubules (Fig. 6H; supplementary material Movie 14), suggesting that *dia* has no essential function in Cip4-induced membrane dynamics.

CIP4 inhibits Dia-dependent actin nucleation and elongation

Finally, we tested whether Cip4 binding affects the actin polymerization activity of the C-terminal half of Dia (DiaC)

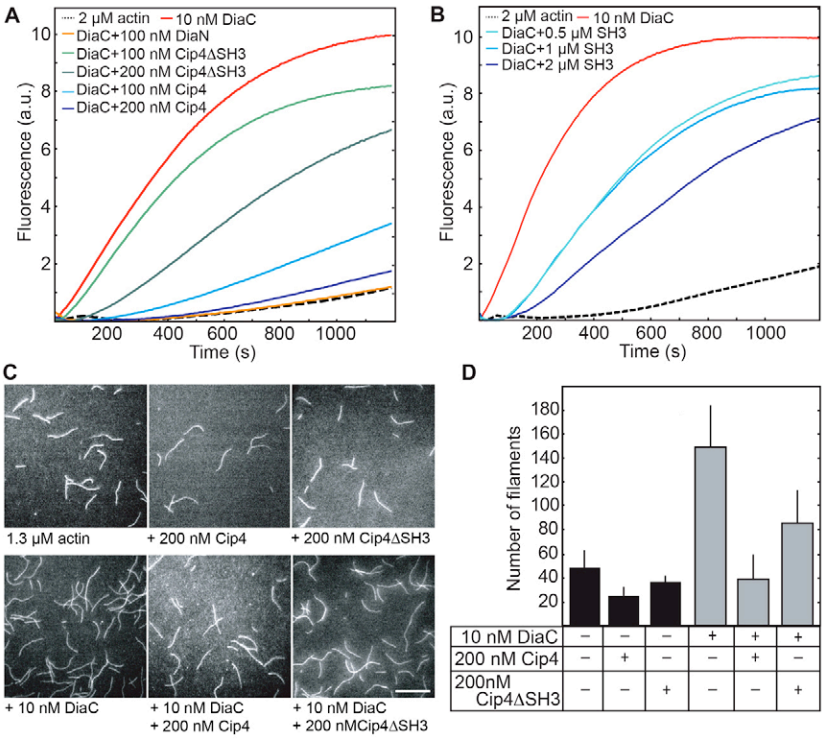

Fig. 7. Cip4 inhibits actin polymerization by Dia. (**A**,**B**) Polymerization of actin (2 μM, 10% pyrene-labelled) in the presence or absence of DiaC, DiaN, Cip4 Cip4ΔSH3 and GST-SH3 at the concentrations indicated. Similarly to the inhibition of DiaC by DiaN, Cip4 inhibits actin polymerization by DiaC in a concentration-dependent manner. Normalized curves are shown. (**C**,**D**) Cip4 and Cip4ΔSH3 inhibit DiaC-mediated nucleation in the absence of profilin, as visualized by TIRF microscopy using 1.3 μM actin (23% Atto488-labelled). (C) Single images of representative time-lapse movies captured 7 minutes after initiation of the experiments. Scale bar: 20 μm. (D) Quantification of nucleated actin filaments after 7 minutes (mean of at least three experiments). Error bars indicate s.d.

that is sufficient for actin nucleation *in vitro* (Grosshans et al., 2005). Consistent with our previous finding (Grosshans et al., 2005), autoinhibition was reconstituted in pyrene assays by addition of ZZ-tagged DiaN, a truncated Dia comprising the N-terminal half (Fig. 7A; supplementary material Figs S3, S4). To test whether Cip4 was able to effect actin assembly, we added increasing amounts of purified Cip4 protein to 10 nM ZZ-DiaC. This led to an inhibition of actin polymerization in a concentration-dependent manner almost comparable to autoinhibition. Notably, a Cip4 mutant protein lacking the C-terminal SH3 domain (Cip4ΔSH3) showed only weak inhibition, indicating that the inhibition of actin polymerization by DiaC is largely mediated by the interaction between the CIP4-SH3 domain and the FH1 domain of Dia. Consistently, GST-SH3 also inhibited actin polymerization, however only at higher concentrations (Fig. 7B). To elucidate whether the inhibition is due to a reduced nucleation activity, filament nucleation was analyzed by *in vitro* TIRF microscopy (Fig. 7C,D; supplementary material Movie 15). 10 nM ZZ-DiaC nucleated approximately three times more filaments when compared to the actin control. Consistent with the pyrene assay, the nucleation activity of DiaC was strongly inhibited by Cip4. Addition of a tenfold molar excess of Cip4 led to the formation of a reduced number of filaments comparable to the actin control. Notably, Cip4ΔSH3 showed a weaker inhibitory effect than full-length Cip4, once more demonstrating the importance of the SH3 domain for the Cip4-Dia interaction. We therefore reasoned that Cip4-SH3 might compete with profilin-actin for binding to the Dia-FH1. In order to allow usage of relatively high concentrations of Cip4, the BAR domain was deleted, since full-length Cip4 formed aggregates above 500 nM at the conditions of the actin polymerization assays. In pyrene assays with DiaC and profilin, Cip4ΔBAR as well as GST-SH3 inhibited actin polymerization (Fig. 8A). Interestingly, the inhibitory effect by the GST-SH3 domain was stronger in the presence of profilin (compare Fig. 7B with Fig. 8B), in fact supporting a competition between profiling–actin and Cip4-SH3 for interaction with Dia-FH1. Like in the absence of profilin (Fig. 7) the nucleation activity of DiaC was inhibited by Cip4ΔBAR and also by Cip4ΔBARΔSH3, albeit to a weaker extend as revealed by the TIRF assay (Fig. 8C).

Formins typically promote actin polymerization not only by their nucleation activities, but also by catalyzing the elongation of existing filament-barbed ends in the presence of profilin. Thus, we next analyzed the elongation properties of DiaC in the absence or presence of regulatory proteins in the TIRF assay. Notably, even in the absence of profilin, DiaC slightly increased the filament elongation rate by about 2 subunits/second to ~16 subunits/second when compared with the actin control elongating with ~14 subunits/second (supplementary material Table S1 and Fig. S6). This was not expected, since all as yet characterized formins inhibit filament elongation under these conditions, albeit the inhibition of fast formins such as mDia1 is negligible (Kovar et al., 2006). Dia certainly belongs to the latter category, as in the presence of profilin, DiaC promoted barbed-end elongation with a speed of ~140 subunits/second (Fig. 8D; supplementary material Table S1). Concerning DiaC-mediated elongation in the presence of profilin and Cip4, two populations of filaments could be identified: fast-growing filaments elongating with about 100 subunits/second and slow-growing filaments that grew like the control filaments with about 11 subunits/second (Fig. 8D–F; supplementary material Table S1). The number of fast-growing filaments was strongly reduced in the presence of Cip4ΔBAR and also by Cip4ΔBARΔSH3, however, only Cip4ΔBAR weakly reduced the elongation rate of the fast-growing filaments. These observations indicate that Cip4 interferes with both Dia activities, though inhibition of nucleation seems to be the main cause.

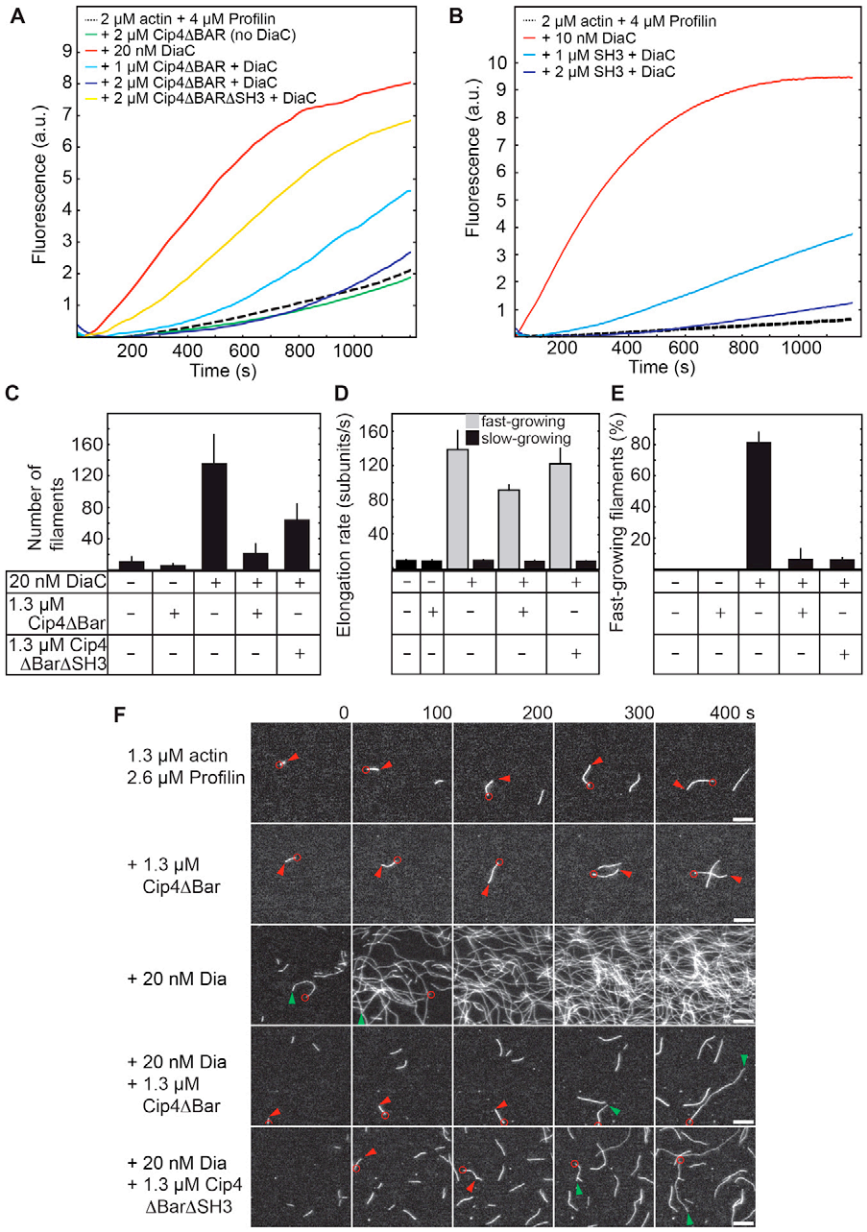

Fig. 8. Cip4 inhibits Dia-mediated filament nucleation and elongation in the presence of profilin. (**A**,**B**) Polymerization of actin (2 µM, 10% pyrene-labelled, and 4 µM profilin) in the presence or absence of DiaC, Cip4ΔBAR, Cip4ΔBARΔSH3 and GST-SH3 at the concentrations indicated. Normalized curves are shown. (**C–F**) Analyses of actin assembly by single filament TIRF microscopy. 1.3 µM actin (23% Atto488-labelled) and 2.6 µM profilin were used in the presence or absence of the Dia and Cip4 constructs at the concentrations indicated (see supplementary material Table S1 for details). (C) Quantification of filament nucleation after 3 minutes. The mean of at least three measurements is shown. Error bars indicate s.d. (D) Elongation rates of growing actin filaments (in actin subunits/second); 15–20 filaments of at least three independent assays were analyzed. Black bars indicate slow-growing filaments that elongate with the speed of actin control filaments and grey bars depict fast-growing filaments. Error bars indicate s.e.m. (E) Proportion of fast-growing filaments after 3 minutes. Error bars indicate s.d. (F) Single frames of representative time-lapse recordings are shown. Red circles mark pointed end of filaments, red arrowheads track barbed ends of slow-growing filaments, and green arrowheads mark barbed ends of fast-growing filaments. Scale bars: 10 µm.

Discussion

A link of F-actin with membrane remodelling and endocytosis is well established (Suetsugu and Gautreau, 2012; Robertson et al., 2009; Itoh et al., 2006; Tsujita et al., 2006). F-BAR proteins recruit activators of the Arp2/3 complex such as WAVE and WASP to endocytic sites (Ho et al., 2004; Takano et al., 2008). Cip4 is one member of the F-BAR protein family (Fricke et al., 2009; Fricke et al., 2010; Nahm et al., 2010) and involved in the control of Arp2/3-dependent actin polymerization and Dynamin recruitment (Fricke et al., 2009). During endocytosis actin filaments stabilize the neck of the endocytic bud, promote efficient budding by Dynamin and displace the budded vesicles away from the membrane (Robertson et al., 2009; Ferguson et al., 2009). In addition to the defined role of F-BAR proteins in linking branched F-actin and endocytosis, F-BAR domain proteins have been found to interact with formins as well, although the relevance of these interactions has remained elusive (Aspenström et al., 2006; Chan et al., 1996). Here, we uncovered a novel interaction of Cip4 with Dia. The function of linear F-actin nucleated by Dia appears to be different from Arp2/3-induced branched F-actin that promotes endocytosis. Dia counteracts membrane remodelling, since *dia* mutants lack the stabilization of the membrane in the basal domain during cellularization as observed by two indicators of membrane stability, tubular extensions labelled by Amph and GFPslam dynamics. The suppression of tubular extensions after about 5 to 10 minutes during wild-type cellularization correlates with the increased stability of the basal domain as measured by membrane labelling (Lecuit and Wieschaus, 2000) and the accumulation of F-actin at the furrow canal. The Cip4-induced tubules in cultured S2R+ cells are, however, unrelated to the Amph-labelled tubular extensions at the furrow canal, since they are budding and not labelled by Amph (data not shown). Thus, Cip4 antagonistically controls two different pools of actin filaments, induction of branched filaments through its WASP/WAVE interaction and suppression of linear filaments formed by Dia. Such

a dual activity may promote efficient membrane remodelling by positively acting on branched F-actin filaments while concomitantly suppressing inhibitory linear actin filaments.

How could Dia suppress tubular membrane extensions? We favour a model in which linear actin filaments form a dense cortical layer that affects the mechanical properties of the membrane such as tension and rigidity. The increased rigidity would make invaginations and bending that can lead to endocytic buds or long membrane extensions less favourable. Such a function would be in contrast to the function of Arp2/3 nucleated branched F-actin network, which has a direct and promoting role in the endocytic reaction cycle. The model is consistent with our previous observation of extracellular blebs within the FC in *dia* mutants (Grosshans et al., 2005), and the data shown here regarding tubular membrane extensions.

Our biochemical analyses revealed unique properties of Dia. As opposed to other formins (Kovar et al., 2006), in the absence of profilin, DiaC even slightly promotes filament elongation. Moreover, by elongating filament barbed ends with ~140 subunits/second in the presence of profilin, Dia is to our knowledge the fastest as yet characterized formin *in vitro*. We further show that Dia interacts with Cip4 leading to inhibition of Dia-mediated actin polymerization. This interaction is primarily based on the Dia-FH1 and Cip4-SH3 domains. In addition to these interacting modules there is also a contribution by other regions outside the SH3 domain, as evidenced by the weak but clear inhibitory effect of Cip4 constructs lacking this region. In bulk actin polymerization assays and by single filament TIRF microscopy we could dissect how Cip4 interferes with Dia function. Cip4 clearly inhibits the nucleation activity, since fewer filaments were formed in the absence or presence of profilin. Cip4 also appears to impair Dia-mediated elongation. Interestingly, however, in the presence of profilin and Cip4ΔBAR, we observed two different populations of filaments. One group comprising the large majority of the filaments (>90%) elongated with the speed of actin control filaments with about 11 subunits/second. The remaining filaments grew with about 66% of the speed of the fast growing filaments in the presence of DiaC and profilin. How can these findings be explained? Cip4 binding to Dia may prevent association of the formin with the barbed end. In this case the filaments would grow as if Dia were not present. The fast growing filaments on the other hand are expected to carry Dia at their barbed ends. However, since these filaments grow slower than the fast Dia control filaments, Cip4 must interfere with their elongation. Cip4-SH3 binding to Dia may therefore, for instance by steric hindrance, either prevent efficient recruitment of actin monomers to the Dia-FH1 region or their subsequent delivery to the catalytic FH2 domain. Alternatively, Cip4 binding may induce structural changes in the FH2 domain. Thus, single molecule imaging combined with multi-colour labelling and structural analysis of the Cip4-Dia complex will be necessary to clearly distinguish these possibilities. *In vivo*, the association of the F-BAR domain with the membrane is also expected to modulate the interaction. Future biochemical studies, including lipid surfaces binding to the F-BAR domain and single molecule experiments with differentially labelled components, will be required to resolve the underlying molecular mechanism at high resolution.

Materials and Methods

Genetics

dia[SY5] was isolated in a screen for novel *dia* alleles (supplementary material Fig. S5). Briefly six alleles (*dia[SY1]* to *dia[SY6]*) were isolated in a F2 screen for lethals over the deficiency Df(2L)DS9 and non-complementation with *dia[1]* out of about 5000 EMS mutagenized *al dp b pr* Frt2L[40A] chromosomes. Transgenes of UASp-GFPslam was generated by P element mediated insertion into the genome by standard techniques. UASp-GFPCip4 and UASp-GFPCip4ΔSH3 transgenes were targeted to the 86Fb (nt 7634081) landing site by PhiC31 (Bischof et al., 2007). Maternal expression of UASp transgenes was driven with a tubulinVP16-GAL4 line (Wenzl et al., 2010). Maternal expression of GFPslam rescues the *slam* cellularization phenotype of Df(2L)BSC5 (data not shown). The following mutations and transgenes were used: *dia[5]* (Afshar et al., 2000), *cip4* (Fricke et al., 2009), *Abl[4]* (Grevengoed et al., 2003), *Arp3* (Berger et al., 2008), UASt-diaRNAi (Vienna stock center. Vdrc stock no. 20518 on III. chromosome), UASt-tubulinGFP, Histon2Av-RFP, UASt-Cip4[Myr]. The myristylation signal was derived from the N-terminal 88 amino acids of the Drosophila *src1* gene and fused in frame with the *Cip4* coding sequence. If not otherwise noted, genetic elements and materials are described in FLYBASE and stocks were obtained from the Bloomington stock centre.

Molecular genetics

UASp-GFPslam: the coding sequence of a GFPslam fusion and the 3′UTR of slam were excised as an XbaI fragment from pMT-GFPslam (Wenzl et al., 2010) and ligated into the XbaI site of pUASp. pETchick was generated by inserting the complete and unchanged coding sequence of *chickadee* (Drosophila profilin, EST clone LD15851) into the NcoI site of pET15b with InFusion technology (Clontech). Cloning primers were AAGAAGGAGATATACCATGAGCTG-GCAA and GATTACTTGCGGGTACTAGCATGGGCAGCAGCCAT. pGST-Amph(1–357) and pUASt-GFPDiaΔDAD plasmids were obtained from Dr O'Kane (Razzaq et al., 2001) and Dr Schejter, respectively. *Cip4* and *dia* cDNAs were amplified by PCR and subcloned into Gateway Entry Vectors (pENTR D-TOPO, Invitrogen) according to the manufacturer's instructions (*Escherichia coli* Expression System with Gateway Technology, Invitrogen). QuickChange XL Site-Directed Mutagenesis (Stratagene, Agilent Technologies) kit was used to generate distinct deletions. Primer details are available upon request. The inserts were sequenced and cloned into corresponding destination vectors (Drosophila Genomics Resource Center) by LR *in vitro* recombination, containing UASt/p promoters and C-terminal eGFP and Cherry tags. dsRNA was synthesized by *in vitro* transcription with T7 RNA polymerase with PCR amplified DNA (Wenzl et al., 2010). The following primers were used to generate a *dia* specific template: TAATACGACTCACTATAGGGTCGTTCTGCATTGTCTA-TGAGC and TAATACGACTCACTATAGGGATCTTCTTCTCGTACTCCTCCG.

An overview of Dia and Cip4 constructs is summarized in supplementary material Fig. S3.

Histology

Embryos were fixed either in 4% formaldehyde/PBS or heat treatment and methanol as previously described (Wenzl et al., 2010). The following antibodies were used: rabbit-anti-Dia (1:1000, Grosshans et al., 2005), rabbit-anti-Slam (1:2000, Wenzl et al., 2010), mouse-anti-Dlg (1:100, Hybridoma Center), mouse-anti-Arm (1:200, Hybridoma Center), rabbit-anti-Patj (1:1000, Richard et al., 2006), rabbit-anti-Cip4 (1:500, preadsorbed at *Cip4* deficiency embryos, Fricke et al., 2009), guinea pig- and rat-anti-Amph (1:1000). Secondary antibodies were labelled with Alexa dyes (4 µg/ml, Invitrogen) or Atto dyes (1:100, for STED). F-actin was stained by Alexa-phalloidin (Invitrogen) and DNA was stained using DAPI (0.2 µg/ml). The Amph antibodies were raised against GST-Amph (aa 1–357). GST-Amph protein was expressed in *E. coli* and purified by chromatography with GSH-Sepharose (GE Healthcare) beads.

Microinjection of embryos

Microinjection was performed as previously described (Grosshans et al., 1994). Alexa-labelled wheat germ agglutinin was injected into the perivitelline space of embryos in nuclear cycle 13. Arp2/3 inhibitor CK666 (Nolen et al., 2009; in DMSO, Calbiochem) into the posterior half of embryos. Fixation was about 15 minutes after injection. The estimated injection volume is assumed to be in the range of 1% of the total embryo volume.

Imaging of embryos

Preparation and handling of embryos for life imaging was as previously described (Kanesaki et al., 2011). Time-lapse movies were recorded with a spinning disc confocal microscope (Zeiss ObserverZ1 with CSU-X1, AxioCam MR camera, Plan Apochromat 25×, NA 0.5, Plan NeoFluar 40× oil, NA 1.3). GFPslam dynamics fluorescent images of fixed and immunostained embryos were recorded with a Zeiss LSM780 (LCI Plan-Neofluar 63× glycerol NA 1.3) and a Zeiss LSM510 (Plan-Apochromat 63× oil, NA 1.4). STED microscopy was performed with custom-made equipment (S. Hell, Max-Planck-Institute Göttingen). Images were processed with Fiji/ImageJ and Adobe Photoshop. Amph tubules extending from the furrow canal were scored with images covering 20 to 40 FC. The proportion of the furrows with at least one Amph tubules was calculated. *P*-values were calculated by Student's *t*-test.

Time-lapse observation of living pupal wing cells

Each pupa was placed on double-sticky scotch tape, and the pupal case was completely peeled off with forceps and put on a 35-mm glass-bottomed dish (MatTek) with the wing epithelium down. The pupae were supported by wet filter paper to prevent desiccation. The dish was sealed with PARAFILM. GFP/Cherry signals were imaged with a confocal spinning disc microscope (PerkinElmer).

Preparation of adult wings

Wings were dissected from adult flies and mounted in a 1:1 mixture of Canada Balsam and methyl salicylate. Brightfield images were acquired using a Zeiss Axiophot microscope and the Zeiss Axiovision image capture software. Auto-Montage Essentials software (Syncroscopy) was used to automatically combine the in-focus region from a series of original images into a single montaged image.

Cell culture and transfection

Drosophila S2R+ cells were cultured and transfected as described previously (Bogdan et al., 2005). For confocal spinning-disc imaging microscopy, transfected cells were replated on chambered cover glass (Lab-Tek) pretreated with ConcavalinA (0.5 mg/ml; Sigma). Image sequences were processed with FIJI/ImageJ. GFP-DiaΔDAD was expressed by cotransfection of pAct-GAL4 plasmid (actin5C promoter driving GAL4). The dia RNAi experiment was performed with a S2R+ cell line stably expressing Cip4-GFP (Fricke et al., 2009). DNA in living cells was stained by Hoechst dye.

Immunoprecipitation

Co-immunoprecipitations were performed as described previously (Bogdan et al., 2005).

Biochemistry

Purification of ZZ-Dia(1–519)-His6 (DiaN) and ZZ-Dia(519–1091)-His6 (DiaC) was as described previously (Grosshans et al., 2005). In brief, proteins were expressed in *E. coli* BL21DE with QE80 plasmids with 0.5 mM IPTG at 18℃ overnight. Buffer was 20 mM sodium phosphate pH 8, 500 mM NaCl and 20 mM imidazole for lysis, 40 mM imidazole for washing and 500 mM for elution. GST-Cip4, GST-Cip4ΔSH3 and GST-SH3 were expressed in *E. coli* with 0.5 mM IPTG at 37℃ for 4 hours and purified from the lysate by affinity chromatography with Glutathione sepharose beads (GSTrapHP, GE Healthcare). Following buffers were used: lysis and washing buffer: 50 mM Tris/HCl pH 8.0, 500 mM NaCl, 1 mM DTT, elution buffer, 50 mM Tris/HCl pH 8.0, 500 mM NaCl, 1 mM DTT, 10 mM Glutathion. For SH3 protein NaCl was 100 mM in all buffers. For GST-Cip4 and GST-Cip4ΔSH3 the fusion proteins were cleaved overnight by PreScission protease in dialysis tubing in 2.6× storage buffer without glycerol. The GST moiety was removed by passing the solution over a Glutathione Sepharose column (GSTrapHP, GE Healthcare). The proteins were stored in 20 mM HEPES, 150 mM NaCl, 0.5 mM DTT, 60% Glycerin at −20℃. *Drosophila* profilin was expressed in *E. coli* BL21DE with pETchick (37℃, 0.5 mM IPTG, 4 hours). Protein was purified from the lysate (in P buffer: KCl 100 mM, glycine 100 mM, Tris/HCl 30 mM pH 8.0, DTT 1 mM) by poly-proline affinity chromatography (Kaiser et al., 1989). After extensive washing with P puffer, the protein was eluted by P buffer with 30% DMSO. Following precipitation in 2.4 M ammonium sulfate at 4℃, gel filtration with Superdex75 (16/60) and concentration with vivaspin column (MW5000), the protein was stored in P buffer with 60% glycerol at −20℃. The poly-proline affinity matrix was prepared by coupling 0.25 g of poly-L-proline to 3 g of CNBr-Sepharose (GE Healthcare) in 12 ml 100 mM $NaHCO_3$/NaOH pH 8.3, 300 mM NaCl for 2 hours. After quenching with 0.1 volume of 1 M NaCl, 1 M glycine, 100 mM Tris pH 7.5 and extensive washing with water, the resin was stored in 10 mM Tris/HCl pH 7.5, 50 mM KCl, 1 mM EDTA, 0.002% sodium azide. The analysis of actin polymerization in pyrene assays and by TIRF microscopy was essentially performed as described (Block et al., 2012). In brief, images from an Olympus IX-81 inverted microscope were captured every 2 seconds with exposure times of 100 milliseconds with a Hamamatsu Orca-R2 CCD camera operated at a 2×2 binning mode. For comparison of nucleation efficacies, the average number of filaments was obtained by counting actin filaments in an area of 100×140 µm, 7 minutes (or 3 minutes in presence of profilin) after initiation of the polymerization reaction. Elongation rates were measured by manual tracking the growing filaments using ImageJ (http://rsb.info.nih.gov/ij).

Acknowledgements

We thank C. O'Kane, K. Kapp, S. Luschnig, E. Schejter, A. Sokac, the Developmental Studies Hybridoma Bank at the University of Iowa, the Bloomington Drosophila Stock Center and the Genomic Resource Center at Indiana University for materials and fly stocks.

Author contributions

S.Y., C.W. and Z.L. analysed compartment separation and tubular extensions. S.Y. and Z.L. analysed Cip4 experiments in embryos. J.G. analyzed GFPslam dynamics. S.B. and Z.L. analysed Cip4-Dia interaction *in vitro* and in flies. T.Z. performed the localisation studies in S2 cells. Z.L. and M.W. conducted the actin polymerisation assays. J.G., S.B. and J.F. designed the experiments and wrote the manuscript.

Funding

This work was in part supported by the priority programme 'Actin nucleators' (SPP1464) and an individual grant to S.B. of the German Research Council (DFG). Z.L. was supported by the Chinese Scholarship Council (CSC).

Supplementary material available online at
http://jcs.biologists.org/lookup/suppl/doi:10.1242/jcs.118422/-/DC1

References

Afshar, K., Stuart, B. and Wasserman, S. A. (2000). Functional analysis of the Drosophila diaphanous FH protein in early embryonic development. *Development* **127**, 1887-1897.

Aspenström, P. (2010). Formin-binding proteins: modulators of formin-dependent actin polymerization. *Biochim. Biophys. Acta* **1803**, 174-182.

Aspenström, P., Richnau, N. and Johansson, A. S. (2006). The diaphanous-related formin DAAM1 collaborates with the Rho GTPases RhoA and Cdc42, CIP4 and Src in regulating cell morphogenesis and actin dynamics. *Exp. Cell Res.* **312**, 2180-2194.

Berger, S., Schäfer, G., Kesper, D. A., Holz, A., Eriksson, T., Palmer, R. H., Beck, L., Klämbt, C., Renkawitz-Pohl, R. and Önel, S. F. (2008). WASP and SCAR have distinct roles in activating the Arp2/3 complex during myoblast fusion. *J. Cell Sci.* **121**, 1303-1313.

Bischof, J., Maeda, R. K., Hediger, M., Karch, F. and Basler, K. (2007). An optimized transgenesis system for Drosophila using germ-line-specific phiC31 integrases. *Proc. Natl. Acad. Sci. USA* **104**, 3312-3317.

Block, J., Breitsprecher, D., Kühn, S., Winterhoff, M., Kage, F., Geffers, R., Duwe, P., Rohn, J. L., Baum, B., Brakebusch, C. et al. (2012). FMNL2 drives actin-based protrusion and migration downstream of Cdc42. *Curr. Biol.* **22**, 1005-1012.

Bogdan, S., Stephan, R., Löbke, C., Mertens, A. and Klämbt, C. (2005). Abi activates WASP to promote sensory organ development. *Nat. Cell Biol.* **7**, 977-984.

Campellone, K. G. and Welch, M. D. (2010). A nucleator arms race: cellular control of actin assembly. *Nat. Rev. Mol. Cell Biol.* **11**, 237-251.

Castrillon, D. H. and Wasserman, S. A. (1994). Diaphanous is required for cytokinesis in Drosophila and shares domains of similarity with the products of the limb deformity gene. *Development* **120**, 3367-3377.

Chan, D. C., Bedford, M. T. and Leder, P. (1996). Formin binding proteins bear WWP/WW domains that bind proline-rich peptides and functionally resemble SH3 domains. *EMBO J.* **15**, 1045-1054.

Chesarone, M. A., DuPage, A. G. and Goode, B. L. (2010). Unleashing formins to remodel the actin and microtubule cytoskeleton. *Nat. Rev. Mol. Cell Biol.* **11**, 62-74.

Faix, J. and Grosse, R. (2006). Staying in shape with formins. *Dev. Cell* **10**, 693-706.

Ferguson, S. M., Raimondi, A., Paradise, S., Shen, H., Mesaki, K., Ferguson, A., Destaing, O., Ko, G., Takasaki, J., Cremona, O. et al. (2009). Coordinated actions of actin and BAR proteins upstream of dynamin at endocytic clathrin-coated pits. *Dev. Cell* **17**, 811-822.

Fricke, R., Gohl, C., Dharmalingam, E., Grevelhörster, A., Zahedi, B., Harden, N., Kessels, M., Qualmann, B. and Bogdan, S. (2009). Drosophila Cip4/Toca-1 integrates membrane trafficking and actin dynamics through WASP and SCAR/WAVE. *Curr. Biol.* **19**, 1429-1437.

Fricke, R., Gohl, C. and Bogdan, S. (2010). The F-BAR protein family Actin' on the membrane. *Commun. Integr. Biol.* **3**, 89-94.

Giuliani, C., Troglio, F., Bai, Z., Patel, F. B., Zucconi, A., Malabarba, M. G., Disanza, A., Stradal, T. B., Cassata, G., Confalonieri, S. et al. (2009). Requirements for F-BAR proteins TOCA-1 and TOCA-2 in actin dynamics and membrane trafficking during Caenorhabditis elegans oocyte growth and embryonic epidermal morphogenesis. *PLoS Genet.* **5**, e1000675.

Grevengoed, E. E., Fox, D. T., Gates, J. and Peifer, M. (2003). Balancing different types of actin polymerization at distinct sites: roles for Abelson kinase and Enabled. *J. Cell Biol.* **163**, 1267-1279.

Grosshans, J., Wenzl, C., Herz, H. M., Bartoszewski, S., Schnorrer, F., Vogt, N., Schwarz, H. and Müller, H. A. (2005). RhoGEF2 and the formin Dia control the formation of the furrow canal by directed actin assembly during Drosophila cellularisation. *Development* **132**, 1009-1020.

Grosshans, J., Bergmann, A., Haffter, P. and Nüsslein-Volhard, C. (1994). Activation of the kinase Pelle by Tube in the dorsoventral signal transduction pathway of Drosophila embryo. *Nature* **372**, 563-566.

Heath, R. J. and Insall, R. H. (2008). F-BAR domains: multifunctional regulators of membrane curvature. *J. Cell Sci.* **121**, 1951-1954.

Ho, H. Y., Rohatgi, R., Lebensohn, A. M., Le Ma, Li, J., Gygi, S. P. and Kirschner, M. W. (2004). Toca-1 mediates Cdc42-dependent actin nucleation by activating the N-WASP-WIP complex. *Cell* **118**, 203-216.

Homem, C. C. and Peifer, M. (2008). Diaphanous regulates myosin and adherens junctions to control cell contractility and protrusive behavior during morphogenesis. *Development* **135**, 1005-1018.

Itoh, T., Erdmann, K. S., Roux, A., Habermann, B., Werner, H. and DeCamilli, P. (2006). Dynamin and the actin cytoskeleton coorperateively regulate plasma membrane invagination by BAR and F-BAR proteins. *Dev. Cell* **9**, 791-804.

Kaiser, D. A., Goldschmidt-Clermont, P. J., Levine, B. A. and Pollard, T. D. (1989). Characterization of renatured profilin purified by urea elution from poly-L-proline agarose columns. *Cell Motil. Cytoskeleton* **14**, 251-262.

Kanesaki, T., Edwards, C. M., Schwarz, U. S. and Grosshans, J. (2011). Dynamic ordering of nuclei in syncytial embryos: a quantitative analysis of the role of cytoskeletal networks. *Integr. Biol. (Camb)* **3**, 1112-1119.

Kovacevic, I., Hu, J., Siehoff-Icking, A., Opitz, N., Griffin, A., Perkins, A. C., Munn, A. L., Müller-Esterl, W., Popp, R., Fleming, I. et al. (2012). The F-BAR protein NOSTRIN participates in FGF signal transduction and vascular development. *EMBO J.* **31**, 3309-3322.

Kovar, D. R., Harris, E. S., Mahaffy, R., Higgs, H. N. and Pollard, T. D. (2006). Control of the assembly of ATP- and ADP-actin by formins and profilin. *Cell* **124**, 423-435.

Lecuit, T. and Wieschaus, E. (2000). Polarized insertion of new membrane from a cytoplasmic reservoir during cleavage of the Drosophila embryo. *J. Cell Biol.* **150**, 849-860.

Levayer, R., Pelissier-Monier, A. and Lecuit, T. (2011). Spatial regulation of Dia and Myosin-II by RhoGEF2 controls initiation of E-cadherin endocytosis during epithelial morphogenesis. *Nat. Cell Biol.* **13**, 529-540.

Li, F. and Higgs, H. N. (2003). The mouse Formin mDia1 is a potent actin nucleation factor regulated by autoinhibition. *Curr. Biol.* **13**, 1335-1340.

Massarwa, R., Schejter, E. D. and Shilo, B.-Z. (2009). Apical secretion in epithelial tubes of the Drosophila embryo is directed by the Formin-family protein Diaphanous. *Dev. Cell* **16**, 877-888.

Nahm, M., Kim, S., Paik, S. K., Lee, M., Lee, S., Lee, Z. H., Kim, J., Lee, D., Bae, Y. C. and Lee, S. (2010). dCIP4 (Drosophila Cdc42-interacting protein 4) restrains synaptic growth by inhibiting the secretion of the retrograde Glass bottom boat signal. *J. Neurosci.* **30**, 8138-8150.

Nolen, B. J., Tomasevic, N., Russell, A., Pierce, D. W., Jia, Z., McCormick, C. D., Hartman, J., Sakowicz, R. and Pollard, T. D. (2009). Characterization of two classes of small molecule inhibitors of Arp2/3 complex. *Nature* **460**, 1031-1034.

Padash Barmchi, M., Rogers, S. and Häcker, U. (2005). DRhoGEF2 regulates actin organization and contractility in the Drosophila blastoderm embryo. *J. Cell Biol.* **168**, 575-585.

Razzaq, A., Robinson, I. M., McMahon, H. T., Skepper, J. N., Su, Y., Zelhof, A. C., Jackson, A. P., Gay, N. J. and O'Kane, C. J. (2001). Amphiphysin is necessary for organization of the excitation-contraction coupling machinery of muscles, but not for synaptic vesicle endocytosis in Drosophila. *Genes Dev.* **15**, 2967-2979.

Richard, M., Grawe, F. and Knust, E. (2006). DPATJ plays a role in retinal morphogenesis and protects against light-dependent degeneration of photoreceptor cells in the Drosophila eye. *Dev. Dyn.* **235**, 895-907.

Roberts-Galbraith, R. H. and Gould, K. L. (2010). Setting the F-BAR: functions and regulation of the F-BAR protein family. *Cell Cycle* **9**, 4091-4097.

Robertson, A. S., Smythe, E. and Ayscough, K. R. (2009). Functions of actin in endocytosis. *Cell. Mol. Life Sci.* **66**, 2049-2065.

Seth, A., Otomo, C. and Rosen, M. K. (2006). Autoinhibition regulates cellular localization and actin assembly activity of the diaphanous-related formins FRLalpha and mDia1. *J. Cell Biol.* **174**, 701-713.

Sokac, A. M. and Wieschaus, E. (2008a). Local actin-dependent endocytosis is zygotically controlled to initiate Drosophila cellularization. *Dev. Cell* **14**, 775-786.

Sokac, A. M. and Wieschaus, E. (2008b). Zygotically controlled F-actin establishes cortical compartments to stabilize furrows during Drosophila cellularization. *J. Cell Sci.* **121**, 1815-1824.

Suetsugu, S. and Gautreau, A. (2012). Synergistic BAR-NPF interactions in actin-driven membrane remodeling. *Trends Cell Biol.* **22**, 141-150.

Takano, K., Toyooka, K. and Suetsugu, S. (2008). EFC/F-BAR proteins and the N-WASP-WIP complex induce membrane curvature-dependent actin polymerization. *EMBO J.* **27**, 2817-2828.

Tsujita, K., Suetsugu, S., Sasaki, N., Furutani, M., Oikawa, T. and Takenawa, T. (2006). Coordination between the actin cytoskeleton and membrane deformation by a novel membrane tubulation domain of PCH proteins is involved in endocytosis. *J. Cell Biol.* **172**, 269-279.

Wenzl, C., Yan, S., Laupsien, P. and Grosshans, J. (2010). Localization of RhoGEF2 during Drosophila cellularization is developmentally controlled by Slam. *Mech. Dev.* **127**, 371-384.

Zelhof, A. C., Bao, H., Hardy, R. W., Razzaq, A., Zhang, B. and Doe, C. Q. (2001). Drosophila Amphiphysin is implicated in protein localization and membrane morphogenesis but not in synaptic vesicle endocytosis. *Development* **128**, 5005-5015.

Journal of Cell Science

Supplementary material. Yan et al., 2013

Table S1: Number of and elongation rates of actin filaments.

Reaction conditions	Number of filaments		Fast-growing filaments			Elongation rate in subunits/s	
	N	S.D.	P (in %)	S.D.		v	S.D.
1.3 µM actin+ 2.6 µM Profilin	11.5	6.66	0	0		11.71	1.77
+ 1.3 µM Cip4ΔBar	6.66	3.51	0	0		10.75	0.82
+ 20 nM DiaC	136.67	37.90	81.53	6.66	fast-growing	138.78	23.09
					slow-growing	11.07	1.32
+ 20 nM DiaC	22.8	12.56	6.45	7.00	fast-growing	91.99	7.62
+ 1.3 µM Cip4ΔBAR					slow-growing	11.15	0.56
+ 20 nM DiaC	65	20.74	6.16	1.69	fast-growing	122.04	19.99
+ 1.3 µM Cip4ΔBarΔSH3					slow-growing	10.05	1.26

Fig. S1. Endocytosis of extracellular cargo does not depend on *dia*. (A) To visualize endocytosis, fluorescently labelled wheat germ agglutinin (WGA-Alexa555) was injected into the extracellular perivitteline space. (B) Time-lapse recording 20 min after onset of.cellularization with a frame rate of 1 in 3 s. Arrow heads indicate endocytic events in wild type and *dia* embryos. (C) Photographs of WGA555 injected wild type and *dia[SY5]* embryos (frame rate of 1 in 5 min). Fluorescent particles in basal cytoplasm were marked in red. (D) Quantification of basal particles in a given section in each three wild type and *dia[SY5]* embryos. (E) WGA555 (red) injected wild type and *dia[SY5]* embryos fixed and stained for the FC marker Slam (green). Section in large magnification. Scale bar 10 µm. (D).

Fig. S2. Cip4-GFPΔSH3 does not induced cellularization defects. Embryos expressing Cip4-GFPΔSH3 were fixed and stained for (A) GFP (white/green), F-actin (white/red) and DAPI (blue) or (B) Dlg (white/green), Slam (white/red) and DAPI (blue). (A) Surface view and cross section of the same embryo.

Fig. S3. Constructs used in this study. Tags are labelled in grey (ZZ, GST), blue (myc) and green (GFP, Cherry). DiaN and DiaC contained a His6 tag at the C-terminus. The domain structure of Dia (FH3+RBD, FH1, FH2, DAD) is indicated in red, of Cip4 (F-BAR, HR1, SH3), in yellow. Numbers in parentheses indicated the amino acid residues contained in the construct. The Delta sign indicates the amino acid residues lacking in the construct.

Figure S4. Proteins used in this study. Samples of the purified proteins as designated were analysed by SDS polyacrylamide electrophoresis and stained by Coomassie.

Figure S5. *dia* locus and alleles. Exons and coding sequence of *dia* are indicated by boxes and blue shading. Domain structure of Dia protein is indicated by boxes. *dia*[1] is a transposon insertion in the first exon (Castrillon1994). *dia*[5] is a derivative isolated after mobilisation of *dia*[1], which has not been molecularly characterised (Afshar2000). *dia*[SY*n*] alleles were induced by chemical mutagenesis. Point mutations were determined by sequencing of the isogenic chromosomes. Resulting alteration in the sequence of amino acid residues are indicated. *dia*[SY4] and *dia*[SY6] are clonal.

Figure S6. Actin filament elongation rates in the absence of presence of DiaC or Cip4. Analyses of actin assembly by single filament TIRF microscopy. 1.3 µM actin (23% Atto488 labelled) in the presence or absence of the Dia and Cip4 constructs at the concentrations indicated were used. Error bars indicate S.E.M. More than 20 filaments of at least three independent assays were analyzed for each condition.

Supplemental material. Figure S1: Yan et al

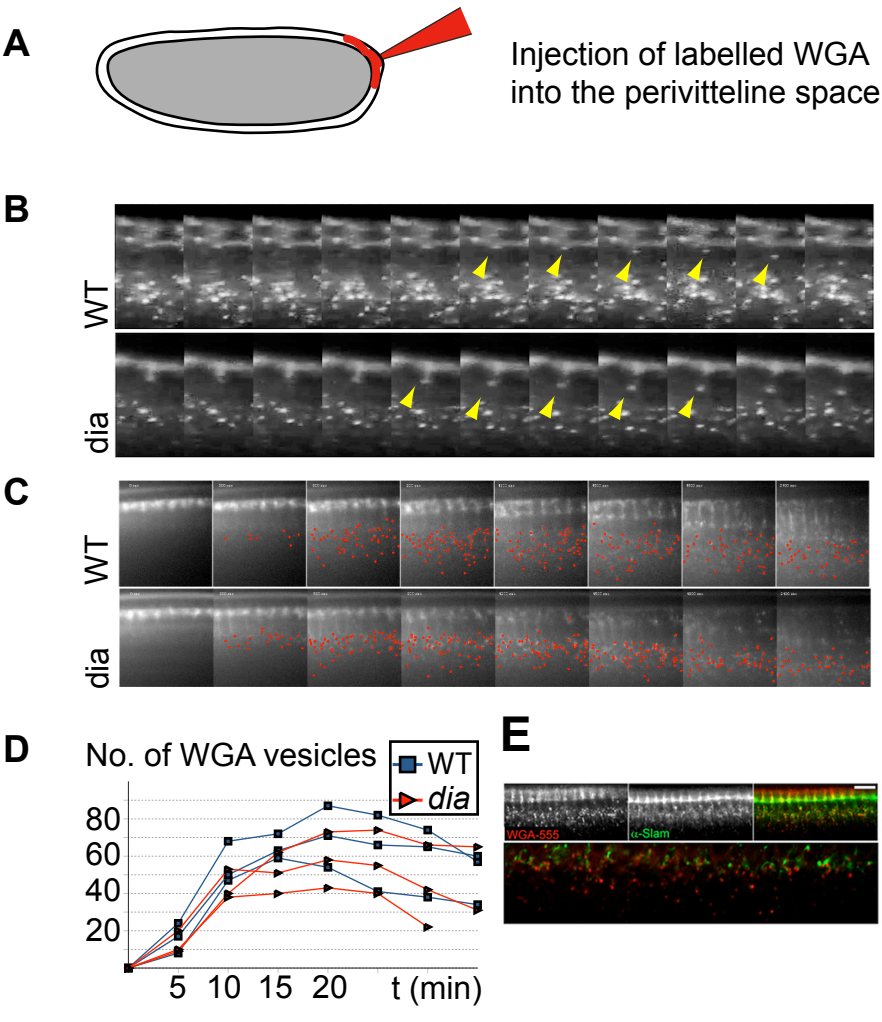

Supplemental material. Figure S2: Yan et al

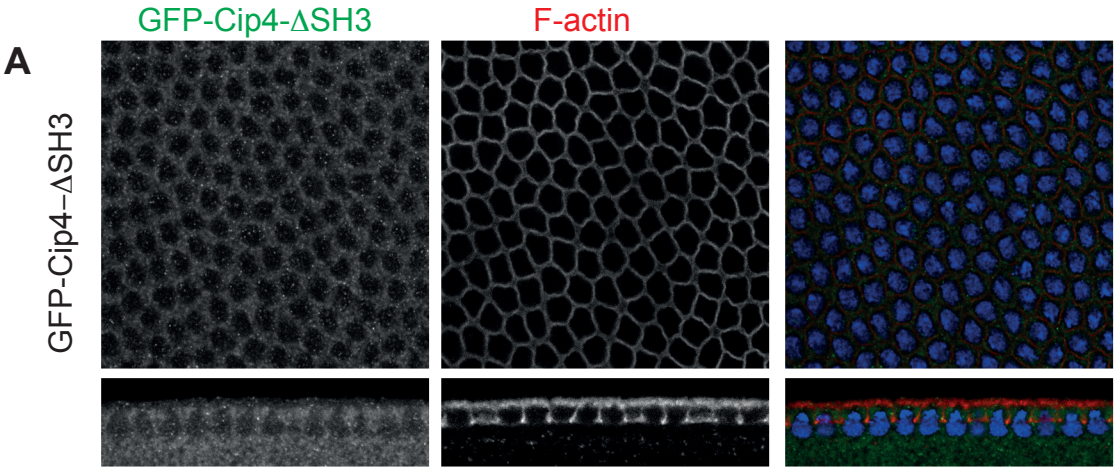

Supplemental material. Figure S3: Yan et al

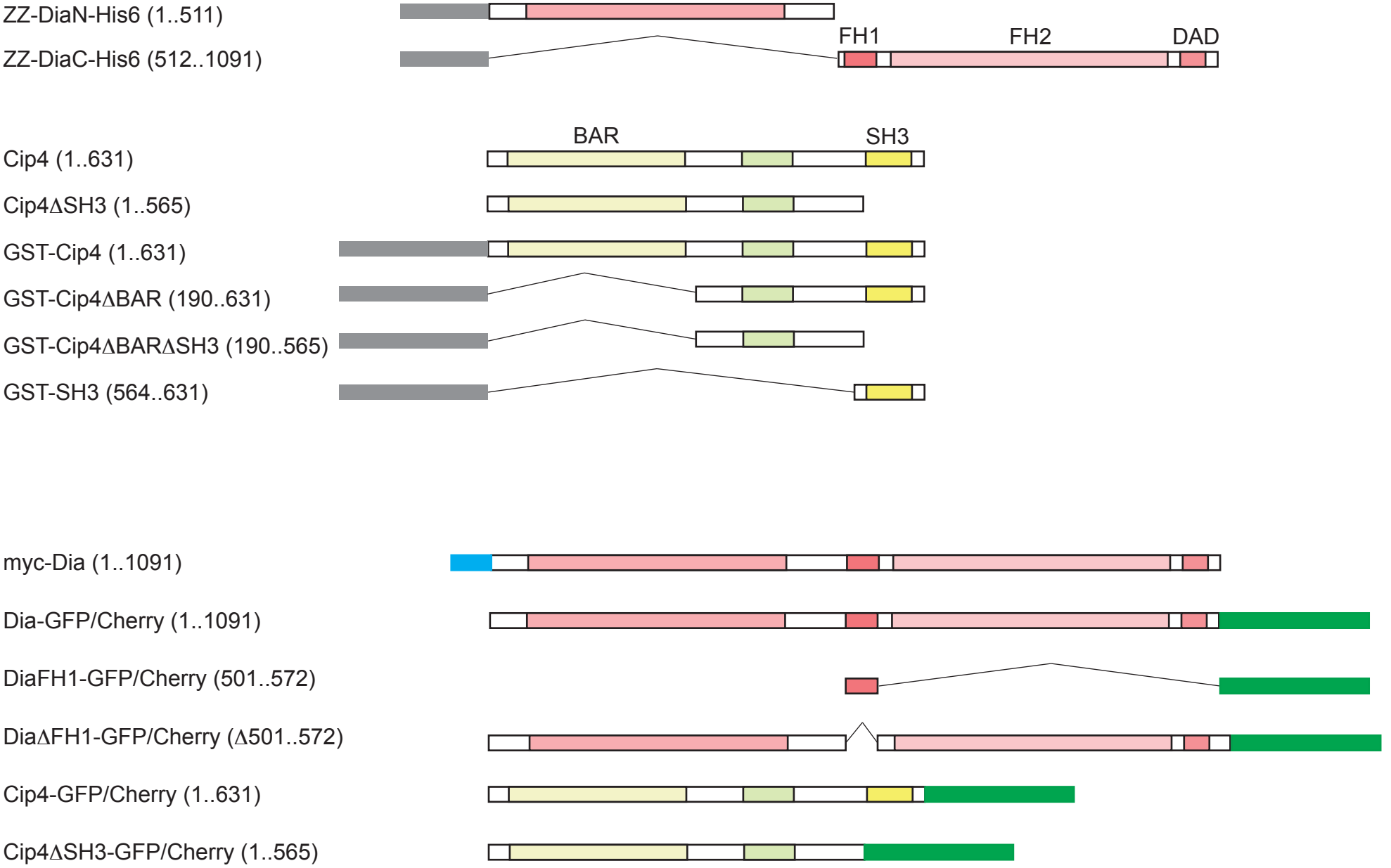

Supplemental material. Figure S4: Yan et al

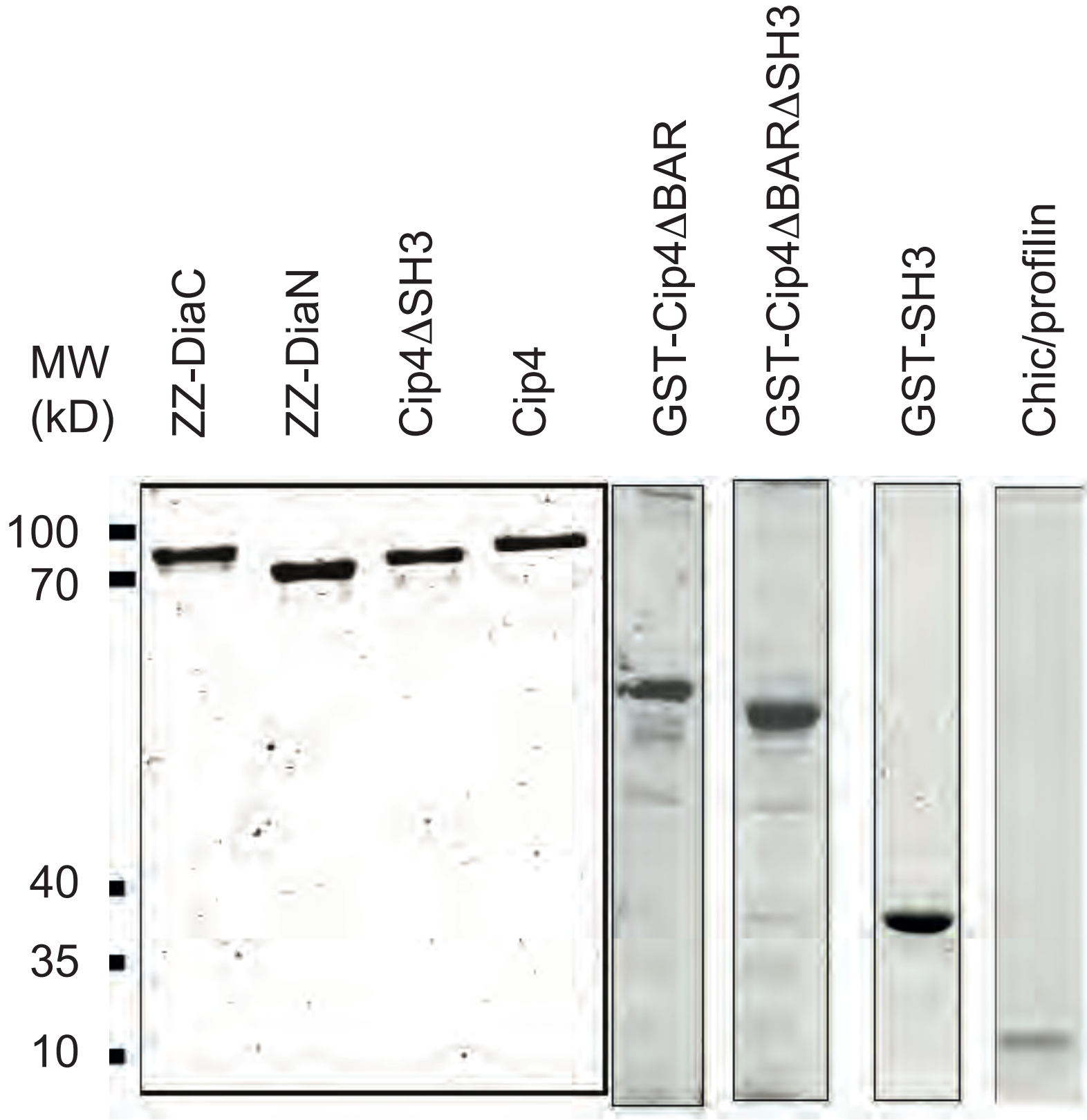

Supplemental material. Figure S5. Yan et al

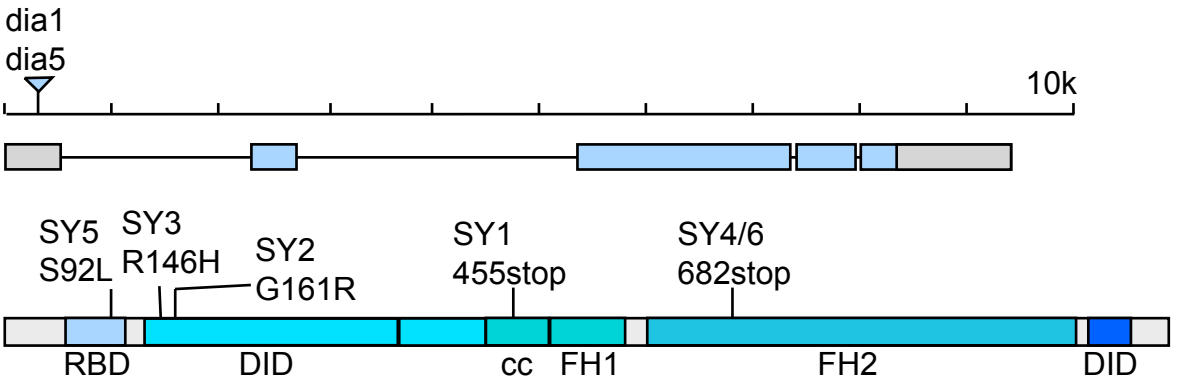

Supplemental material. Figure S6

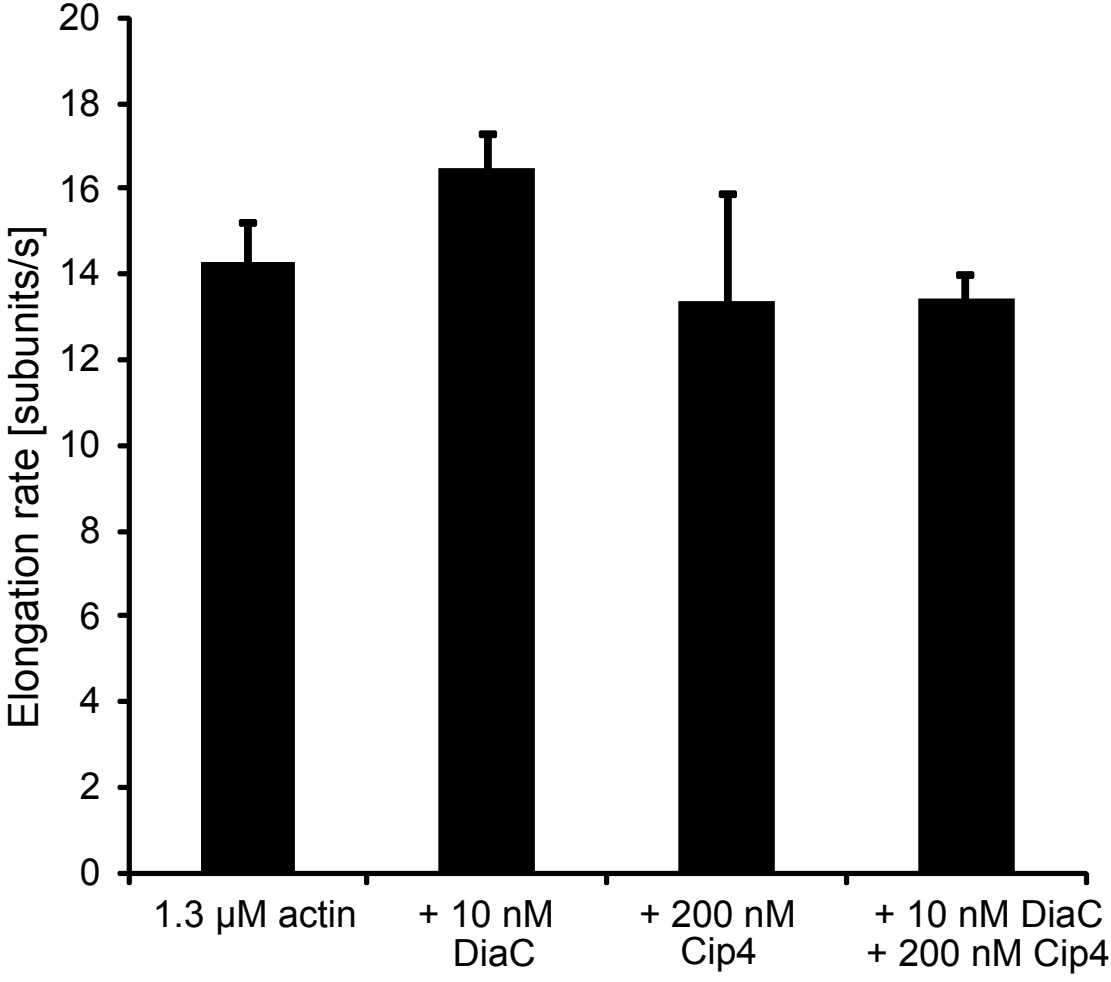

Movie 1. GFPslam in wild type embryo. GFPslam labels the basal domain of the metaphase furrow in mitosis and the furrow canal in interphase 14. Dynamical membrane extensions are observed in mitosis and initial interphase 14. In telophase 13 and progressively in interphase 14 the extensions disappear. Frame rate 1/5s, pixel size 130 nm, focal depth 50-60 µm. The time lapse recording shows the dynamics of GFPslam from interphase 13 to interphase 14.

Movie 2. GFPslam in *dia*[SY5] embryo. In *dia* embryos the metaphase furrows do not form properly and the furrow canals that form are often severely dilated. The dynamical membrane extensions remain visible throughout cellularization. GFPslam is expressed maternally by a tubulinVP16 GAL4 driver line. Frame rate 1/5s, pixel size 130 nm, focal depth 50-60 µm. The time lapse recording shows the dynamics of GFPslam from interphase 13 to interphase 14.

Movie 3. WGA endocytosis in wild type embryo. Frame rat 1/3s. The time lapse recordings show the incorporation of fluorescent protein (wheat germ agglutinin-Alexa555) injected into the extracellular perivitteline space. Note that endocytic particles appear all along the furrow.

Movie 4. WGA endocytosis in *dia[SY5]* embryo. Frame rat 1/3s. The time lapse recordings show the incorporation of fluorescent protein (wheat germ agglutinin-Alexa555) injected into the extracellular perivitteline space. Note that endocytic particles appear all along the furrow.

Movie 5. Wild type wing imaginal disc, GFP-tubulin, Histone2Av-RFP.

Movie 6. Wing imaginal disc expressing Cip4[myt], GFP-tubulin, Histone2Av-RFP.

Movie 7. Wing imaginal disc expressing *dia* RNAi, GFP-tubulin, Histone2Av-RFP. The time lapse recordings show the mitotic cells in wing imaginal discs recognizable by the chromosome dynamics labelled by Histone2Av-RFP. During cytokinesis the separation of the daughter cells is marked by the labeling of microtubules. In cell lacking cytokinesis two nuclei share a common arrangement of microtubules.

Movie 8. S2 cells expressing Dia-GFP, DiaΔFH1-GFP, or DiaFH1-GFP.

Movie 9. S2 cells expressing full length Dia-GFP and Cip4-Cherry.

Movie 10. S2 cells expressing full length dia-Cherry (green) and Cip4ΔSH3-GFP (red).

Movie 11. S2 cells expressing DiaΔFH1-GFP and Cip4-Cherry.

Movie 12. S2 cells expressing DiaFH1-GFP and Cip4-Cherry.

Movie 13. S2 cells expressing DiaΔDAD-GFP and Cip4-Cherry. S2 cells expressing differentially tagged Dia and Cip4 proteins. Cip4 expression induces tubular invaginations at the plasma membrane and labels intracellular vesicles. The time lapse recordings show the dynamics of the Dia and Cip4 proteins in relation to each other in interphase cells.

Movie 14. S2 cells expressing Cip4-Cherry treated with *dia* RNAi. S2 cells stably expressing Cip4-GFP. Expression of Cip4-GFP was induced 3 days after treatment with *dia* RNAi.

Movie 15. Analysis of actin assembly by single filament TIRF microscopy. Dynamics of actin filaments visualized by fluorescently labelled actin monomers in the presence profilin, DiaC, Cip4ΔBAR, Cip4ΔBARΔSH3 as indicated.